# Directional Spectrum Estimation for Sea States Generated by the Single Summation Method

Iversen, Sarah Krogh; Andersen, Thomas Lykke; Frigaard, Peter

*Published in:*
JOURNAL OF COASTAL AND HYDRAULIC STRUCTURES

*DOI (link to publication from Publisher):*
10.59490/jchs.2024.0036



*Publication date:*
2024

*Document Version*
Publisher's PDF, also known as Version of record

JOURNAL OF COASTAL AND HYDRAULIC STRUCTURES

*Vol.* 4, 2024, 36

# Directional spectrum estimation for sea states generated by the single summation method

Sarah Krogh Iversen[1], Thomas Lykke Andersen[2], and Peter Frigaard[3]

## Abstract

The influence of directional spreading of waves is significant for wave-induced loads, wave breaking and nonlinearity of the waves. For physical model testing performed at test facilities such as the Ocean and Coastal Engineering Laboratory at Aalborg University, it is crucial to validate if the test conditions match the target sea states by measurement and analysis of the generated directional wave field. Most of the existing methods assumes a double summation sea state to be present which is valid in the prototype. However, waves in the laboratory are usually generated by single summation. The current paper presents a method to analyse short-crested waves generated by the single summation method. The present method considers oblique reflections instead of only in-line reflections as assumed in similar existing methods. The results show that the new SORS method successfully decomposes the incident and reflected wave fields in the time domain. Thus, for example the incident wave height distribution may be obtained. The sensitivity of the new method to additional reflective directions, noise, calibration errors and positional errors of the wave gauges was found to be small.

**Keywords:**

Wave Analysis, Directional Spectrum Estimation, Directional Spreading Function, Single Summation Method, Wave Reflection

## 1 Introduction

In the design of coastal and offshore structures, it is important to consider the directionality of the waves. The directionality of the waves will influence wave kinematics, loads on the structures, wave breaking, nonlinearity of the waves and the likelihood of extreme waves. For design of wave energy converters, the directionality might also influence the power production significantly, depending on the type of device. A widely used tool in the design of coastal and offshore structures is physical model testing in wave tank facilities. Analysis of the generated multidirectional wave fields in the model is needed to validate that the target sea states are obtained.

[1]ski@build.aau.dk, Aalborg University, Denmark
[2]tla@build.aau.dk, Aalborg University, Denmark
[3]pf@build.aau.dk, Aalborg University, Denmark

Research Article. **Submitted:** 29 May 2024. **Reviewed:** 17 August 2024. **Accepted** after double-anonymous review: 22 October 2024. **Published:** 02 December 2024.

DOI: https://doi.org/10.59490/jchs.2024.0036

Cite as: Iversen, S. K., Lykke Andersen, T., Frigaard, P. (2024): Directional spectrum estimation for sea states generated by the single summation method, Journal of Coastal and Hydraulic Structures, 4, 36, DOI: https://doi.org/10.59490/jchs.2024.0036

This paper is part of the **Thematic Series** of selected papers on advances in physical modelling and measurement of Coastal Engineering issues, as presented on the Coastlab Conference in Delft in 2024.



ISSN: 2667-047X online

For physical model testing it is common to analyse the short-crested waves from measurements of surface elevation time series in multiple positions. Most existing methods for directional spectrum estimation aim to solve the Directional Spreading Function (DSF) and cover the commonly applied methods; the Bayesian Directional spectrum estimation Method (BDM) (Hashimoto and Kobune, 1988), the Maximum Likelihood Method (MLM) (Capon et al. 1976, Isobe et al. 1984, and Krogstad 1988) and the Maximum Entropy Method (MEM) (Hashimoto et al., 1994). The DSF-based reconstruction methods assume that the wave field is generated by double summation, which means that many directions will be present at each frequency. This will be the case in a natural environment, but for laboratory tests Miles and Funke (1989) recommended to use single summation generation. This means that each frequency has just one generated direction of propagation. Their recommendation was based on the requirement to have a spatially homogeneous incident energy level in the basin.

A comparative analysis of different analysis methods for short-crested waves was performed in Hawkes et al. (1997), from which it was concluded that most of the methods do not detect the reflected wave components very well. Especially for wave fields close to the reflecting structure, where phase-locking will occur. Moreover, most of the methods assume that the DSF is either of a specific shape or at least that it is a smooth function, which is not necessarily the case. For laboratory generated waves the spreading function has to be truncated as otherwise too large spurious waves will be generated due to the discretization of the wavemaker. Moreover, single summation generated sea states do not necessarily have a smooth DSF within each frequency bin analyzed.

When analysing waves in physical model tests, a time domain solution providing the incident wave train is often desired. This is because the response of the structure is usually characterized by time domain parameters including for example the maximum wave height, $H_{max}$, the 2% exceedance probability wave height, $H_{2\%}$, and the significant wave height, $H_{1/3}$. The aforementioned methods only provide spectral parameters. Another type of method has been developed in the present work, which allows a decomposition in the time domain by utilizing the knowledge that a single summation sea state is present. Thus, exactly the generated frequencies are analyzed and therefore the resolution of the analyzed frequency domain is equal to the one used for generation. For a wave field generated by single summation, this will mean that only a single incident direction is present at each generated frequency. It is important to note that analyses of exactly the generated frequencies requires synchronization of the wave generation and acquisition to avoid influence of crystal clock differences. The principles have been applied to multidirectional waves by Draycott et al. (2015) using the original formulations by Esteva (1976). Draycott et al. (2016) showed that the combined wave generation-measurement approach used in the SPAIR method (Single-summation PTPD Approach with In-line Reflections) enables increased certainty in estimation of the incident directional spectra in presence of in-line reflections compared to the DSF-based reconstruction methods, that are inherently associated with some uncertainty. In the SPAIR method by Draycott et al. (2016) an incident wave component is assumed to give rise to a single reflected component in the opposite direction. This is certainly not always valid, but it is valid for a circular wave basin without a structure, for which the SPAIR method was developed. The assumption of in-line reflection allows for the separation of the incident and reflected waves using methods developed for long-crested waves, i.e. Zelt and Skjelbreia (1992), Goda and Suzuki (1976) or Mansard and Funke (1980). The decomposition of long-crested waves has furthermore been extended to include nonlinear effects, as done by i.e. Lin and Huang (2004), Eldrup and Andersen (2019), and Padilla and Alsina (2020). For structures exposed to short-crested waves, the reflected direction is in many cases unknown. When oblique reflections of more than 20° occur, it is not appropriate to use in-line reflection analysis as also demonstrated in Draycott et al. (2016). The present paper will therefore present a method to perform the decomposition in incident and reflected components independent of the directional difference between the two. The new method is named SORS, Single-summation Oblique Reflection Separation.

The method requires the generated incident wave field to be of the single summation model. This will usually yield just one incident and one reflected direction for each frequency component. Other components may be thought to be present due to corner reflection compensation (Dalrymple, 1989), diffraction from one or more models, cross-modes, wall reflections, and nonlinear interactions in the sub and superharmonic regions. Common for these different contributions is that they diverge from the single summation model assumptions. Such contributions are therefore not considered in the mathematical model. Apart from that also calibration errors and measurement uncertainties and noise could be present in the signals. In the present work it will therefore be tested how sensitive the wave decomposition is towards such phenomena. The performance of the method is demonstrated using synthetically generated waves. First, the methodology of the present work will be presented including wave generation and the principles of the method. Next, the sensitivity towards diverging factors will be tested by using synthetically generated data. The performance will be quantified based on how well the incident and reflected time series are estimated. Finally, the stability of the method is briefly discussed along with future potential development of the method.

## 2 The New SORS Method

The use of the SORS method assumes that the wave field is generated from the single summation method by linear wave theory as expressed in Equation (1), where $a_i$ is the amplitude, $k_i$ is the wave number, $\theta_i$ is the direction of propagation, $\omega_i$ is the angular frequency and $\varphi_i$ is the phase shift, all of them of the $i$'th wave component for $i = 0, 1, \ldots N-1$, where $N$ is the total number of frequency components.

$$\eta(x, y, t) = \sum_{i=0}^{N-1} a_i \cos\left[k_i(x\cos\theta_i + y\sin\theta_i) - \omega_i t + \varphi_i\right] \tag{1}$$

It is assumed that there is no interaction between the wave components and that no currents are present, so likewise, there is no wave-current interaction. It is furthermore assumed that the wave field is stationary, that no wave breaking, shoaling, or refraction occurs, and that each angular frequency ($\omega_i = 2\pi f_i$) has just one incident and one reflected wave component, that are not necessarily in line with each other. The above assumptions are applied over the spatial area where Eq. (1) is applied (usually the measurement array). The frequencies in the signal are assumed to be known from the wave generation ($N$ frequencies, $f_i = i \cdot \Delta f, i = 1, 2 \ldots N-1, \Delta f = f_s/N$ ). Acquisition and wave generation needs to be synchronized to avoid differences in sample frequencies ($f_s$) caused by crystal clock variations.

The surface elevation of irregular three-dimensional waves including incident and reflected wave components in position $(x, y)$ can then be described by:

$$\begin{aligned}\eta(x, y, t) = &\sum_{i=0}^{N-1} a_{I,i} \cos\left[k_i(x\cos\theta_{I,i} + y\sin\theta_{I,i}) - \omega_i t + \varphi_{I,i}\right] \\ &+ \sum_{i=0}^{N-1} a_{R,i} \cos\left[k_i(x\cos\theta_{R,i} + y\sin\theta_{R,i}) - \omega_i t + \varphi_{R,i}\right] \\ &+ \text{noise}\end{aligned} \tag{2}$$

where subscripts $I$ refers to the incident wave component and $R$ refers to the reflected wave components. The wave number, $k$, is determined from the linear dispersion relation, where $\omega$ is the frequency of the wave component and $h$ is the water depth:

$$\omega^2 = gk\tanh(kh) \tag{3}$$

The directional analysis is performed one frequency at a time, wherefore $i$ is omitted in the following. The surface elevation in frequency domain, $\hat{\eta}$, can then be described from Equation (4) at each gauge position $m$, where $m = 1, 2 \ldots P$, for the total number of gauges, $P$.

$$\begin{aligned}\hat{\eta}(x_m, y_m) &= C_{I,m}X_I + C_{R,m}X_R + \Omega_m \\ X_I &= a_I \exp(-\mathrm{i}\varphi_I) \\ X_R &= a_R \exp(-\mathrm{i}\varphi_R) \\ C_{I,m} &= \exp[-\mathrm{i}k(x_m\cos\theta_I + y_m\sin\theta_I)] \\ C_{R,m} &= \exp[-\mathrm{i}k(x_m\cos\theta_R + y_m\sin\theta_R)]\end{aligned} \tag{4}$$

where $\Omega_m$ is the Fourier transformation of the noise at gauge $m$ and frequency $\omega$. $C_R$ and $C_I$ are here defined based on the absolute phases, wherefore $X_I$ and $X_R$ are the complex wave amplitude of the incident and reflected wave components respectively in position $(x, y) = (0, 0)$. The values of the complex parameters, $X_I$ and $X_R$ are determined by fitting Equation (4) into the measurement at each frequency by minimising the sum of squares of $\Omega_m$ when summing over all gauge positions, which for the present implementation yields the total error, $E$, in Equation (5).

$$E = \sum_m (\Omega_m)^2 = \sum_m (\hat{\eta}(x_m, y_m) - C_{I,m}X_I - C_{R,m}X_R)^2 \tag{5}$$

The total error, $E$, should be minimised with respect to the unknowns $X_I$, $X_R$, $\theta_I$ and $\theta_R$. For a given estimate of $\theta_I$ and $\theta_R$ it can be minimised with respect to $X_I$ and $X_R$ respectively by:

$$\frac{\partial}{\partial X_I}\sum_m(\Omega)^2 = \frac{\partial}{\partial X_R}\sum_m(\Omega)^2 = 0 \tag{6}$$

As consequence of fitting the Fourier coefficients using a least squares approach, a larger number of wave gauges than unknown parameters is preferred, as the reflection analysis benefits from an overdetermined system. The directional analysis in general requires a minimum of 3 wave gauges. Adopting the notation by Lin and Huang (2004), the equations for solving for the two unknown parameters $X_I$ and $X_R$ in Equation (6) can be written as:

$$\begin{bmatrix} A_{11} & A_{12} \\ A_{21} & A_{22} \end{bmatrix} \begin{bmatrix} X_I \\ X_R \end{bmatrix} = \begin{bmatrix} B_1 \\ B_2 \end{bmatrix} \tag{7}$$

The elements of $A_{ij}$ and $B_i$ are given by:

$$A_{11} = \sum_m (C_{I,m})^2$$

$$A_{12} = \sum_m (C_{I,m}C_{R,m}) = A_{21}$$

$$A_{22} = \sum_m (C_{R,m})^2$$

$$B_1 = \sum_m [\hat{\eta}(x_m, y_m)C_{I,m}]$$

$$B_2 = \sum_m [\hat{\eta}(x_m, y_m)C_{R,m}]$$

where $\hat{\eta_m}$ is the Fourier coefficients of the surface elevation data in wave gauge position $m$. To separate the incident and reflected components, it is thus here assumed that the incident and reflected directions, $\theta_I$ and $\theta_R$, are known, which is the case for long-crested waves. In order to find the best estimate for the directions $\theta_I$ and $\theta_R$ for each frequency component, the error is initially calculated for a mesh of direction combinations. A range for the incident directions and reflected directions are defined, such that the analysis seeks for incident components in a specified range and for reflected components in another specified range as exemplified in Figure 1. The resolution of the mesh is 2°.

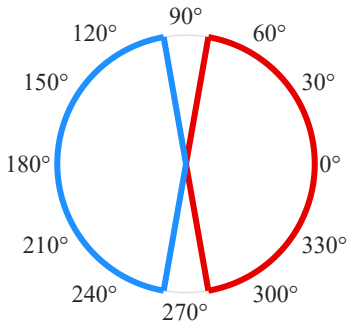


Figure 1: Pre-specified ranges for incident (red) and reflected (blue) wave components.

For each of the given incident and reflected directions of propagation $\theta_I = [\theta_{I,min}; \theta_{I,max}]$ and $\theta_R = [\theta_{R,min}; \theta_{R,max}]$, the linear system of equations in Equation (7) is solved which yields the isolated complex parameters $X_I$ and $X_R$ with a least-square error, $E$, determined based on the difference between the estimated and measured Fourier coefficients at all gauge positions as stated in Equation (5). The computation is repeated for all combinations of directions in the ranges of incident and reflected directions. The combination of directions yielding the lowest error, $E$, according to the least-squares method is then used as a first estimate. Next, the error, $E$, is minimised with respect to the incident and reflected directions, $\theta_I$ and $\theta_R$, using the Nelder-Mead simplex algorithm (Nelder and Mead, 1965) as implemented in *fminsearch* in MATLAB, from which $X_I$ and $X_R$ in each iteration is calculated by solving the system of equations in Equation (7). The procedure is repeated for all frequency components.

The incident and reflected wave fields can then be reproduced in time domain in wave gauge position $m$, or another adjacent position, by Fast Fourier Transform of the decomposed Fourier coefficients stated in Equation (8) and (9).

$$\hat{\eta}_I(x_m, y_m) = C_{I,m}X_I \tag{8}$$

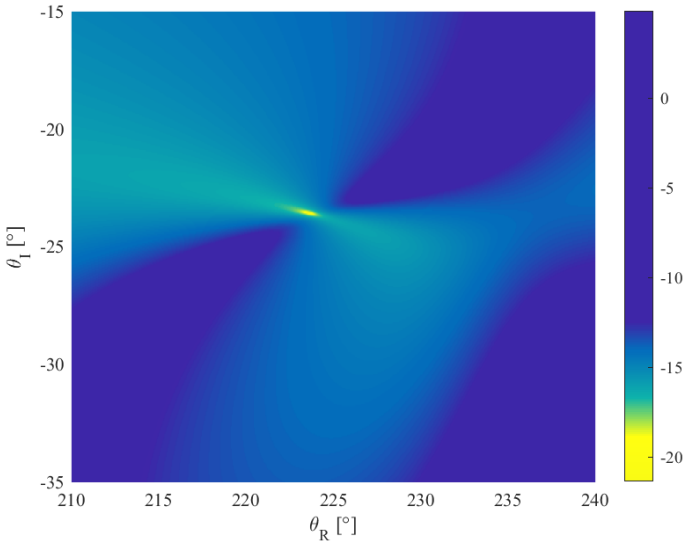


Figure 2: Total error, $E$, for arbitrary wave component as function of incident, $\theta_I$, and reflected, $\theta_R$, directions. Shown in logarithmic scale for full visualisation of behaviour for a range of directions, so $\log(E)$.

$$\hat{\eta}_R(x_m, y_m) = C_{R,m} X_I \tag{9}$$

From the decomposed coefficients, the timeseries can also be reproduced from summation as stated in Equation (2). The amplitudes are then determined as the absolute values of $X_I$ and $X_R$ respectively. The present application uses the fft implemented in MATLAB, which yields the phases $\varphi = \tan^{-1}(-B/A)$, where $A$ is the real part of $X_I$ and $X_R$ respectively and $B$ is the imaginary part. The directional spectrum can be estimated following the same procedure as described by Draycott et al. (2016).

## 2.1 Directional settings

During the analysis, the total error, $E$, is calculated for the full mesh of combinations. The trend for the squared error, $E$, for all frequencies is that a very local minimum occurs for the correct combination of incident and reflected directions. An example of how the total error, $E$, is distributed over the two directions of estimation, $\theta_I$ and $\theta_R$, is illustrated in Figure 2 for an arbitrary frequency component. The full behaviour of the total error is shown in logarithmic scale in Figure 2.

In the process of choosing an appropriate discretization of the directions, the behaviour of the total error is important to consider. The choice of the discretization will be a compromise between accuracy of the initial estimates and the computational time. If the discretization is too coarse, the risk is that local minima will be found in the following optimisation. The consequence of a too coarse grid for the initial mesh is shown in Figure 3, where the estimated reflected direction is seen to be highly influenced by even small errors on the incident direction. In the example studied 30% reflection at angle 223.5˚is present in the wave field.

Different mesh discretization for the initial estimates have been investigated through the development of the method, and at present stage 2˚-intervals are used as it rarely leads to a local minimum instead of the global to be found.

# 3 Test Data

To test the performance of the SORS decomposition method a series of sea states were generated synthetically. Synthetic data was also used to test sensitivity to deviations from the mathematical model due to wall reflections, noise, calibration errors and errors in position of wave gauges.

## 3.1 Sea States and Gauge Array

To test the performance of the decomposition method, a set of sea states with different peak periods corresponding to 1:20 scale of a natural environment at the northwestern coast of Denmark is used. The sea states are generated on

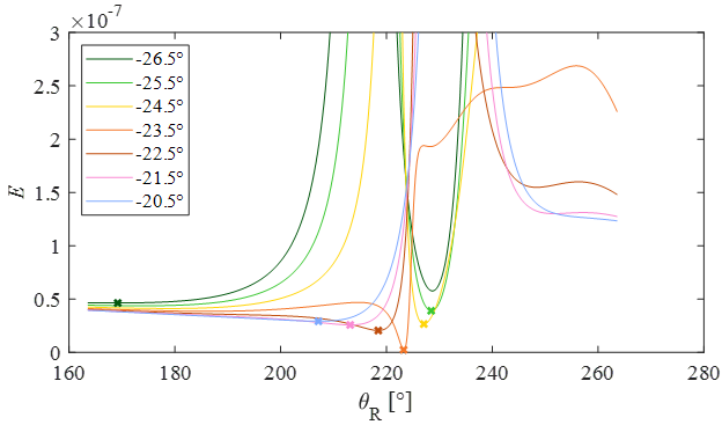


Figure 3: Total error, $E$, as function of the reflected direction, $\theta_R$, for estimations of the incident direction, $\theta_I$, in the range around the correct value of 23.5°.

a water depth $h = 0.715$ m. All sea states are generated from a JONSWAP spectrum with peak enhancement factor $\gamma = 3.3$. The directional parameters of the sea states are defined by the mean wave direction $\theta_0 = 0°$ and a cos-2$s$ spreading function with spreading given by the parameter $s = 10$. The reflections are given by a reflection coefficient, $C_r = 0.3$, and an angle of the reflecting structure, $\alpha_s = 10°$. In the present analyses, the structure is placed at a reference point given in a $x$-distance of 6 m from the point of origin $(0, 0)$. The origin corresponds to an approximate position of the corner of the basin, which is placed outside Figure 4. The wavemakers are placed in line $x = 0$ m.

An overview of the different sea states and the corresponding significant wave parameters are given in Table 1. The present method is developed for wave characterisation in laboratory facilities, wherefore the frequency span is limited to 0.15 Hz – 3 Hz, which is a typical range of generation in physical model testing. The present work uses surface elevations from a standard CERC5 wave gauge array as seen in Figure 4, as it is a commonly applied wave gauge array for wave analysis of multidirectional waves, as the internal directions between the gauges are widely spread. The size of the array is adjusted to each sea state, such that the diameter, $D_{\text{array}} = 2R$, is 0.15 times the wavelength of the peak frequency ($L_p$).

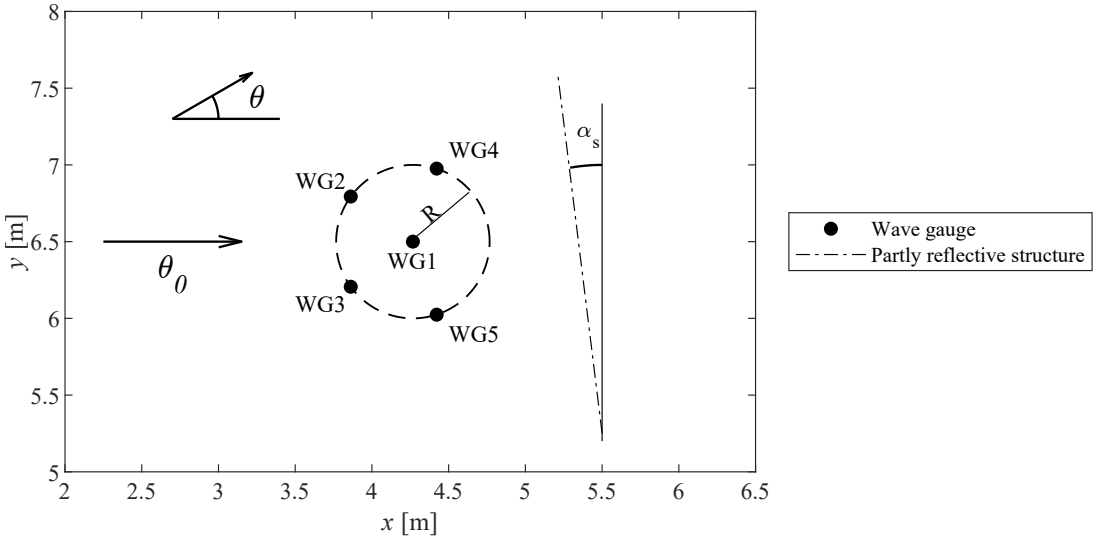


Figure 4: CERC5 wave gauge array.

The present work considers wave fields generated from linear wave theory. The significant wave heights and peak periods in Table 1 are in some of the sea states close to the limit of the applicable range of linear wave theory. If those tests are generated in a physical model then nonlinear waves will appear and these will contribute with larger errors, as demonstrated for long-rested waves by Eldrup and Andersen (2019). As the present work revolves around synthetically generated waves only, it is though not of influence for the analysis, as the generated waves matches the assumptions of the mathematical model in Eq. (1).

| Sea State | $H_{m0}$ [m] | $T_p$ [s] | $L_p$ [m] | $D_{\text{array}}$ [m] |
|---|---|---|---|---|
| 1 | 0.05 | 1.25 | 2.34 | 0.35 |
| 2 | 0.10 | 1.56 | 3.33 | 0.50 |
| 3 | 0.15 | 1.88 | 4.30 | 0.65 |
| 4 | 0.20 | 2.19 | 5.22 | 0.78 |
| 5 | 0.25 | 2.50 | 6.11 | 0.92 |

Table 1: Sea State Parameters

### 3.2 Wave Generation

The present work revolves around the analysis of multidirectional wave fields generated from the single summation model. This means that each generated frequency component has a single direction. As described in the previous section, waves with a directional spreading function as suggested by Mitsuyasu et al. (1975) will be considered, with the directional spreading function, $D(\theta)$, given in terms of the mean wave direction, $\theta_0$, and spreading parameter, $s$, as stated in Equation (10).

$$D(\theta) = \frac{2^{2s-1}\Gamma^2(s+1)}{\pi\Gamma(2s+1)} \cos^{2s}\left(\frac{\theta-\theta_0}{2}\right) \tag{10}$$

Where the double summation generation method would generate several components at the same frequency representing the directional spreading function in Equation (10), the single summation method assumes only one direction for each frequency component. The individual directions are chosen by Monte Carlo simulation of the probability density function of the directional spreading function, $D(\theta)$. A uniformly distributed random number between 0 and 1 is generated for each frequency. The random number will then represent the non-exceedance probability of the directional distribution function, which will be assigned to the component. The surface elevation, $\eta$, in position $(x, y)$ at time $t$ can then be calculated from Inverse Fast Fourier Transform (IFFT) or from summation as described by Equation (1). The phase of each component ($\varphi_i$) is chosen by picking a uniformly distributed random number between $-\pi$ and $\pi$. The single summation method accounts for wave generation in physical tank testing as well as generation of synthetic waves. For the synthetic wave fields, which are analysed in the present work, a reflected wave field is similarly generated. The directions and phases of the reflected components are calculated from a specified distance to a reflecting structure with a specified angle. This reproduces thus a wave field with phase locking in front of the structure.

## 4 Results

The performance of the method can be evaluated based on different parameters depending on the desired application of the analysis. For use in physical model testing of offshore structures, the aim is often to validate the generated sea state and its kinematics and correlate it to measured wave loads on the tested model. Therefore, the performance of the method is here evaluated based on how well the incident and reflected time series of the surface elevation are reproduced by the method. First, a wave field which fully satisfies the assumptions of the presented method is analysed. In section 5, the robustness of the method will be demonstrated towards tank testing phenomena such as wall reflections, noise, calibration error, etc.

As the waves of the present analyses are synthetically generated without errors, the target total time series are identical with the 'measured' time series. An example of the results of the analyses appears in Figure 5, where a segment of the time series of the surface elevation in position of WG1, cf. Figure 4, for sea state 1, cf. Table 1, with 30% reflection is shown. Using the presented method, the incident and reflected time series are accurately reproduced, with error signals with maximum 0.2% of the variance of the original signal. The combined surface elevation of the incident and reflected wave field are illustrated as the total estimated surface elevation, which is seen to match the 'measured' and, in this case, therefore also the target value accurately.

The synthetic generation of the waves also allows for a direct comparison of the target incident and reflected components with the prediction by the method. From Figure 5 it is seen that the decomposed time series also match the target values very well, with a variance in the error signals relative to the target of 0.04% for the incident and 0.05% for the reflected waves taken as the mean over all gauge positions.

As the analysis is performed for all generated frequency components in the spectrum, the values of the individual wave component parameters can also be investigated further. The individual estimated wave component

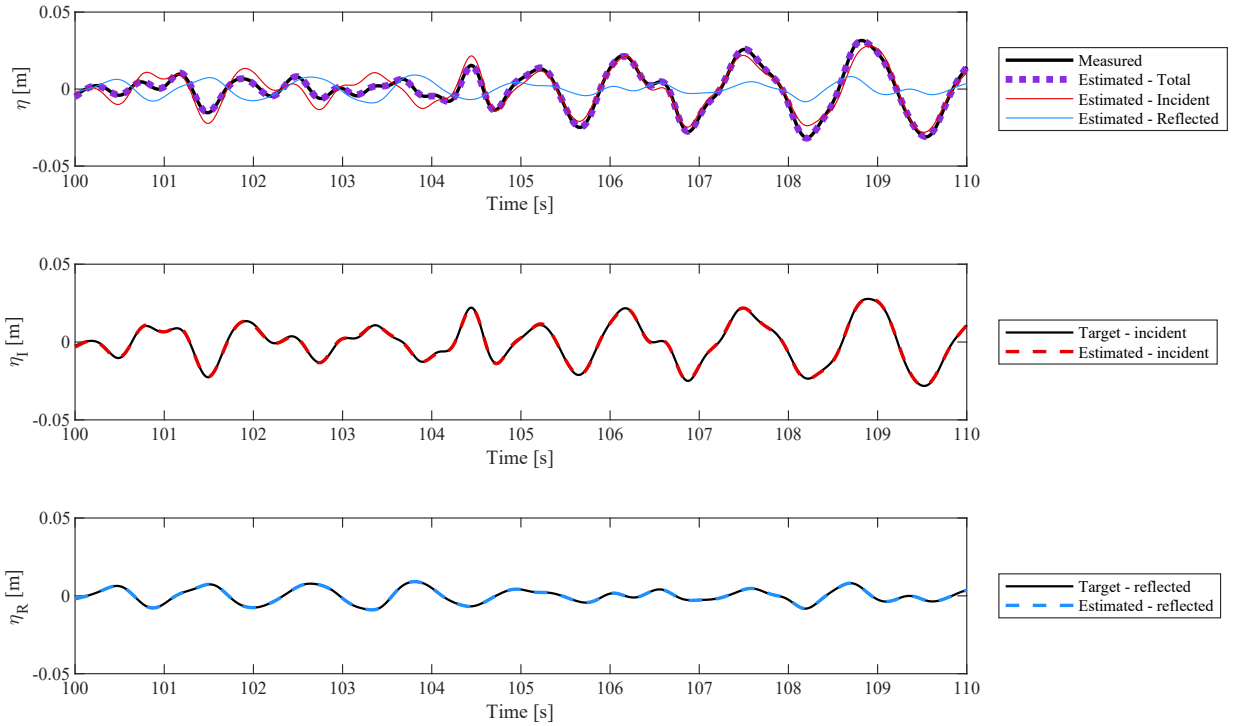


Figure 5: Time series of measured surface elevation (here synthetically generated) and result from the analysis, Sea State 1. Decomposed wave fields compared to target time series are also included.

parameters of this specific sea state are compared to the target values as $\Delta\theta = \theta_{est} - \theta_{target}$ for the direction, $\Delta a/a = (|X_{est}| - |X_{target}|)/|X_{target}|$ for the amplitude, $\Delta\varphi = \varphi_{est} - \varphi_{target}$ for the phase and $E_{rel} = E/\sum_m \hat{\eta}_{target}$ for a relative estimate of the total error over all gauges compared to the energy of the specific component. The values are calculated for the total, incident and reflected components as relevant. The errors on each frequency component appear from Figure 6.

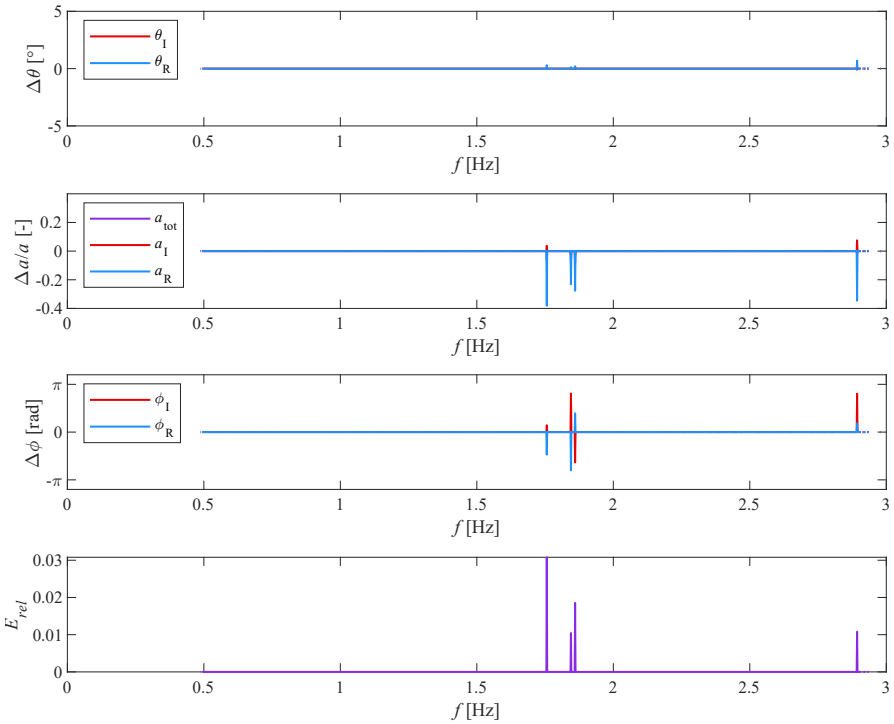


Figure 6: Error on estimated wave component parameters compared to target values for Sea State 1 ($f_p = 0.8$ Hz).

From Figure 6 it appears that the accuracy of the estimation is very high. On few high-frequent components, small

deviations on the estimated amplitudes and phases are present. One reason for the reduced accuracy of the high frequency components can be the design of the gauge array, as the wavelengths of these components become too small for the present array design.

For in-line reflection analysis, it is recommended that the wave gauge distances are in the range of 0.05-0.45 times the wavelength, as shown by Goda and Suzuki (1976). The distances between the gauges in the present array depend on the direction of propagation of the specific component, the number of gauge separations that fulfill this requirement will therefore vary with frequency, due to the wavelength, as well as the direction of propagation. The number of valid gauge separations for the CERC5 array given in Figure 4 is illustrated in Figure 7, where the array is scaled to sea state 1, such that the diameter $D = 0.15L_p$, where $L_p$ is the wavelength of the peak frequency, which is the same sea state as the previous results.

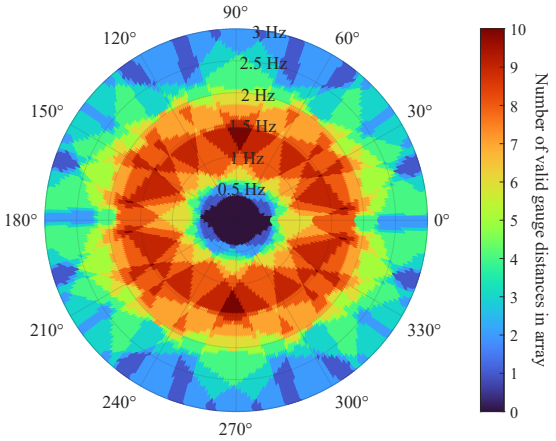


Figure 7: Gauge distances in the CERC5 array scaled to sea state 1, that satisfy the criteria $0.05L < \Delta x_\theta < 0.45L$, where $\Delta x_\theta$ is the distance between two gauges in the direction of propagation of the wave component, illustrated as function of the direction [°] and frequency [Hz].

Another way to determine if the gauge array is useful and an accurate solution to the linear system of equations exists, is based on the condition number as suggested by de Ridder et al. (2023). Based on the estimated incident and reflected directions, the condition number is determined as the 2-norm condition number given by Demmel (1987) as the maximal singular value divided by the minimum singular value of the phase difference matrix, $Z$:

$$Z = \begin{bmatrix} C_{I,1} & C_{R,1} \\ \vdots & \vdots \\ C_{I,m} & C_{R,m} \end{bmatrix} \tag{11}$$

For the same sea state as used in Figure 6, the condition number of the estimated incident and reflected directions for the CERC5 wave gauge array appears from Figure 8 for all frequency components in the analysed spectrum. Similar results are found for the other sea states, indicating that an accurate solution exists for the relevant frequencies and directions for all sea states. Thus, the CERC5 array has a sufficient amount of wave gauges with acceptable distance between them for the present analyses. The layout of the wave gauge array therefore does not yield any limitations to the method. No upper limit, $C_{max}$, is determined for the present analyses, as it does not seem to increase significantly at any point.

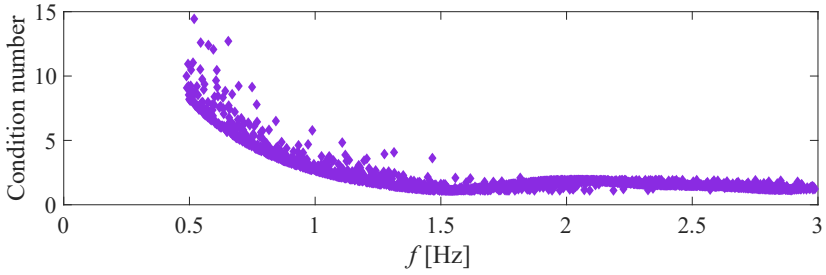


Figure 8: Condition number based on estimated incident and reflected wave directions using the CERC5 array, Sea State 1.

From visual inspection of the time series in Figure 5, the method accurately decomposes wave fields that strictly follow the assumptions. The performance of the method is further quantified based on the variance of the difference between the estimated surface elevation and the target as stated in Equation (12). The analyses are performed for all sea states as given in Table 1.

$$\Delta\sigma^2 = \mathrm{Var}(\eta_{est} - \eta_{target}) \tag{12}$$

The results are presented as the average error over all frequencies and all wave gauge positions in Figure 9 and results are summarised in Table 2.

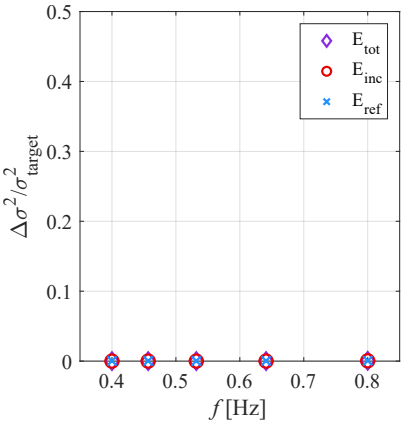


Figure 9: Error on estimated time series.

| Sea State | $E_{tot}$ | $E_{inc}$ | $E_{ref}$ |
|---|---|---|---|
| 1 | 0.04 % | 0.04 % | 0.05 % |
| 2 | 0.00 % | 0.00 % | 0.03 % |
| 3 | 0.00 % | 0.00 % | 0.02 % |
| 4 | 0.00 % | 0.00 % | 0.03 % |
| 5 | 0.00 % | 0.00 % | 0.03 % |

Table 2: Variance error on estimated time series compared to target.

From Table 2 it appears that the higher the peak frequency, the higher the error on the time series. For the sea states with the higher peak frequency, the wavelengths within for instance half to two times the peak frequency has a larger relative difference than the spectra with the lower frequencies. In such case the size and design of array is of influence despite being scaled in size for each of the sea states in the present analyses.

# 5 Discussion

## 5.1 Sensitivity to errors

The sensitivity of the method will then be tested towards factors that cause measurements to deviate from the mathematical model in Equation (2). First, it is tested how additional reflected components, stemming from for instance basin wall reflections behind or beside the structure, more than one model in the basin etc., will affect the decomposition of the wave fields. The same wave fields as the ones yielding the results in Figure 9 are tested, which means that it includes all five sea states given in Table 1 with 30% reflection. Apart from this, additional 10% reflection from the back wall of the wave tank is included. The back wall of the basin is placed perpendicular to the $x$-axis 8m from the wavemakers. The results in Figure 10 show the error on the reconstructed time series taken as the mean over all wave gauges, where it from the error on the incident wave field, $E_{inc}$, is seen that the estimation of the incident wave field is almost unaffected by the additional reflected components. $E_{ref}$ is a comparison of the estimated reflected wave field and the target reflected wave field from the structure only, where it is apparent that the estimated reflection is highly affected by an additional wall reflection. The error on the sum of the structure and wall reflection is given by $E_{ref+wall}$ which is seen to be significantly smaller than $E_{ref}$. For cases where the difference in direction between the wall reflections and reflections from the structure is larger, the error on the reflected wave field is expected to be

higher. If the reflection coefficient is larger than in the present example, then an additional reflected direction might also influence the estimated incident direction.

For the sensitivity towards noise, white Gaussian noise is added to wave fields with a signal-to-noise ratio of 50:1 of the energy. As seen from Figure 11, the method is fully robust towards noise on the signals when sufficient number of gauges are applied.

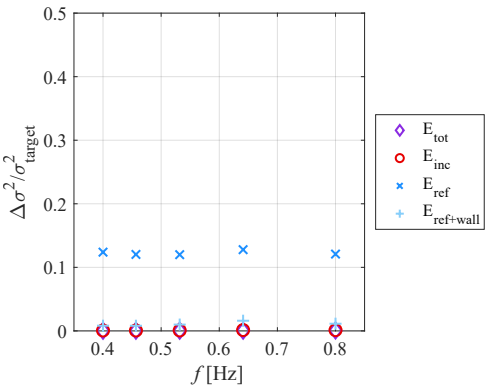


Figure 10: Error on estimated time series, back wall reflection.

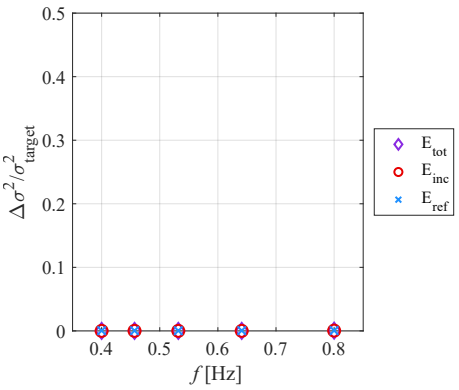


Figure 11: Error on estimated time series, noise.

The following part of the sensitivity analysis revolves around positioning errors of wave gauges where three different configurations (errors) have been tested:

- WG3 moved 0.03m in the $x$-direction
- WG3 moved 0.03m in the $y$-direction
- WG2 moved 0.03m in the $x$-direction and WG3 moved 0.03m in the $y$-direction.

These results appear from Figure 12, where it is seen that the method is very robust towards small inaccuracies in position of the wave gauges. The incident wave field is almost unaffected by the positional error, possibly due to the relatively larger amount of energy, whereas a small increase in the error is seen on the reflected part of the spectrum. Furthermore, the behaviour of the error as function of the frequency is more like the general pattern seen for the full spectrum analyses in Figure 11, that the larger the peak frequency, the lower accuracy is experienced.

Another type of measurement error could be calibration errors. Two different configurations of possible calibration errors are tested:

- 10% gain on WG2
- 10% gain on WG2 and -10% on WG4

The results appear from Figure 13. As the analysed wave fields contain 30% reflection, it is natural that the relative error on the reflected wave field is larger than on the incident wave field. Overall, it can be concluded, that the calibration errors can be rather critical for estimation of the reflected wave field, but less critical for the incident components, which are of primary interest. This conclusion might be different if more gauges were affected by calibration errors.

## 5.2 Separation accuracy

The method is structured in the way that a first estimate of the incident and reflected components of each frequency component is calculated from a mesh of different directions, wherefrom the combination yielding the lowest total error on the Fourier coefficients is chosen as initial estimates. The mesh is defined based on ranges for the incident and the reflected directions to be defined in agreement with the test conditions. A small gap between the incident and reflected sectors must be present for stability of the method. The size of this gap has in the present partly been based on the condition number. In Figure 14 the condition number with respect to the reflected wave direction $\theta_R$ for an incident wave direction of $\theta_I = 0$°is illustrated. As seen from Figure 14, the condition number increases significantly when the two angles are close to each other, indicating that no accurate solution of the wave decomposition exists.

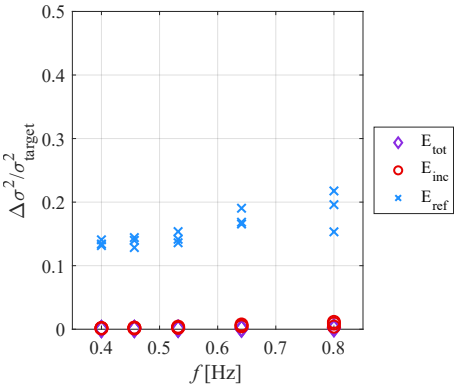


Figure 12: Error on estimated time series, wave gauge position error.

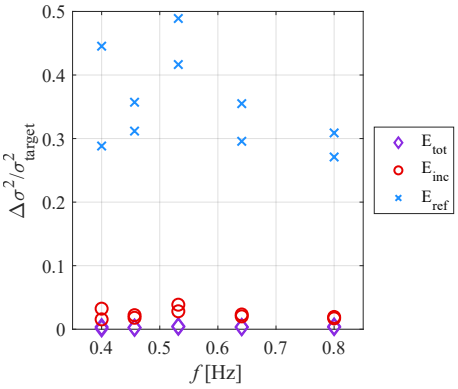


Figure 13: Error on estimated time series, wave gauge calibration error.

Therefore, the initial ranges of the incident and reflected from Figure 1 are chosen such that a gap of 20 degrees exist between them. It could be considered to choose different directional gaps depending on the different frequencies. From Figure 14 it also appears that different frequencies will yield different condition numbers when using the same wave gauge array. This is mainly relevant if a very wide spreading of the waves is present. As it is unlikely that the incident and reflected wave components travel in almost the same direction it does not immediately affect the present implementation of the method.

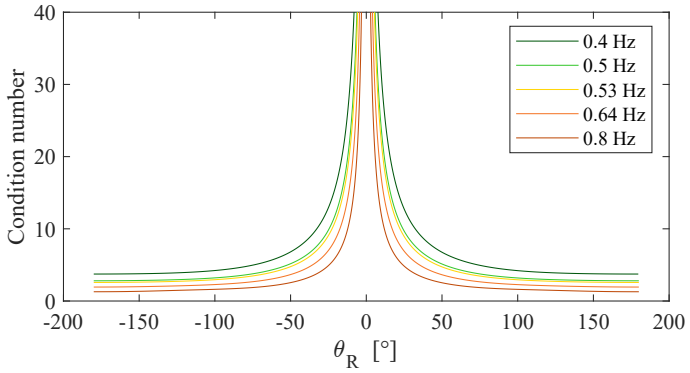


Figure 14: Condition number for CERC5 array as function of reflected direction of propagation, $\theta_R$, for incident wave direction $\theta_I = 0$°for relevant frequencies corresponding to peak frequencies of the investigated sea states.

In general, Wenneker and Hofland (2014) suggests using the condition number to design the gauge array. However, the design process is not as straightforward when dealing with multidirectional waves, which is also supported by Figure 7, where the directional variation of the valid gauge distances appears. Gauge array design for decomposition of multidirectional waves should therefore be investigated further. The gauge array for analysis of multidirectional waves is often designed based on the co-array or lag-array, which describes the internal distances of the wave gauges (Haubrich 1968, Davis and Regier 1977), for which the considerations regarding reflection analysis is however not included.

## 6 Conclusions

For physical model testing of coastal and offshore structure exposed to multidirectional waves, identification of the incident wave field is often required to validate if the sea state matches the target conditions. Most existing methods assume double summation sea states and only provide the directional spectrum and not the time domain parameters. The present paper presents a new methodology for wave decomposition of multidirectional waves generated from the single summation method. The new SORS method successfully reconstructs the incident and reflected wave fields in the time domain. The method allows for oblique reflections, which is not yet covered by existing similar methods for single summation sea states. Through analysis of synthetically generated waves, the SORS method is proven to be robust towards noise, wave gauge calibration errors, positional errors of wave gauges, and additional directional components caused by for example basin wall reflections.

As mentioned earlier, further work should include a more detailed design of the wave gauge array for decomposition of multidirectional waves using the present method. Further analysis related to the sensitivity towards calibration errors should investigate the effects from truncation of the spectrum, scaling of the wave gauge array and number of wave gauges applied. Also, an extension for cross-mode identification could be relevant. Apart from that, the sensitivity of the method towards nonlinear effects should be tested. It is expected that the method will behave similarly as other methods when used for analyses of nonlinear wave fields as shown in Iversen et al. (2023). The structure of the presented method will allow for implementation of nonlinear effects as done by Eldrup and Andersen (2019), which will however require further work regarding assumptions about the directionality of the nonlinear components to avoid a drastic increase in computational consumption.

## Acknowledgements

This work was funded by the Danish Energy Agency under The Energy Technology Development and Demonstration Program (EUDP) contract number 64022-1062.

## Author contributions (CRediT)

SKI: Methodology, Conceptualization, Writing - Original Draft, Writing - Review & Editing, Formal analysis, Visualization. TLA: Conceptualization, Writing - Review & Editing, Supervision. PF: Funding acquisition, Writing - Review & Editing, Supervision.

## Data access statement

The data acquired in the study will be made available upon request.

## Declaration of interest

The authors report no conflict of interest.

## Notations

| Symbol | Description | Unit |
|---|---|---|
| $a$ | wave amplitude | m |
| $C$ | phase-difference term | - |
| $C_r$ | reflection coefficient | - |
| $D(\theta)$ | directional spreading function | $\text{rad}^{-1}$ |
| $D_{\text{array}}$ | diameter of gauge array | m |
| $E$ | squared error on Fourier coefficients | $\text{m}^2$ |
| $f$ | frequency | Hz |
| $f_p$ | peak frequency | Hz |
| $f_s$ | sample frequency | Hz |
| $g$ | gravitational acceleration | $\text{m/s}^2$ |
| $h$ | water depth | m |
| $H_{m0}$ | significant wave height | m |
| $k$ | wave number | rad/m |
| $L_p$ | wavelength of the peak frequency | m |
| $N$ | total number of frequency components | - |
| $P$ | total number of gauges | - |
| $R$ | radius of gauge array | m |
| $s$ | spreading parameter | - |
| $t$ | time | s |
| $T_p$ | peak period | s |
| $x$ | x-coordinate | m |
| $X$ | complex wave amplitude | m |
| $y$ | y-coordinate | m |
| $Z$ | phase difference matrix | - |
| | | |
| $\alpha_s$ | orientation of reflective structure | rad |
| $\gamma$ | peak enhancement factor | - |
| $\eta$ | surface elevation | m |
| $\hat{\eta}$ | Fourier transform of surface elevation | m |
| $\theta$ | direction of propagation | rad |
| $\theta_0$ | mean wave direction | rad |
| $\phi$ | phase shift | rad |
| $\omega$ | angular frequency | rad/s |
| $\Omega$ | Fourier transform of noise term | m |

## References

Capon, J., Greenfield, R.J. and Kolker, R.J. (1976). Multidimensional maximum-likelihood processing of a large aperture seismic array. *Proc. IEEE*, **55**, 192–211.

Dalrymple, R.A. (1989). Directional wavemaker theory with sidewall reflection. *Journal of Hydraulic Research*, **27:1**, 23–34.

Davis, R.E. and Regier, L.A. (1977). Methods for estimating directional wave spectra from multi-element arrays. *Journal of Marine Research*, **35 (3)**, 453–477.

de Ridder, M.P., Kramer, J., den Bieman, J.P. and Wenneker, I. (2023). Validation and practival application of nonlinear wave decomposition methods for irregular waves. *Coastal Engineering*, **183**. DOI: https://doi.org/10.1016/j.coastaleng.2023.104311.

Demmel, J.W. (1987). On condition numbers and the distance to the nearest ill-posed problem. *Numerische Mathematik*, **51**, 251–289.

Draycott, S., Davey, T., Ingram, D.M., Day, A. and Johanning, L. (2016). The spair method: Isolating incident and reflected directional wave spectra in multidirectional wave basins. *Coastal Engineering*, **114**, 265–283. DOI: https://doi.org/10.1016/j.coastaleng.2016.04.012.

Draycott, S., Davey, T., Ingram, D.M., Lawrence, J., Day, A. and Johanning, L. (2015). Using a phase-time-path-difference approach to measure directional wave spectra in flowave. *Proceedings of the 11th European Wave and Tidal Energy Conference (EWTEC), Nantes, France.*

Eldrup, M.R. and Andersen, T.L. (2019). Estimation of incident and reflected wave trains in highly nonlinear two-dimensional irregular waves. *Journal of Waterway, Port, Coastal and Ocean Engineering*, **145(1)**. DOI: doi.org/10.1061/(ASCE)WW.1943-5460.0000497.

Esteva, D. (1976). Wave direction computations with three gage arrays. *Proc. Fifteenth Coastal Engng. Conf., Hawaii, USA*, **1**, 349–367.

Goda and Suzuki (1976). Estimation of incident and reflected waves in random wave experiments. *Proceedings of the 15th Coastal Engineering Conference, New York, USA*, 828–845.

Hashimoto, N. and Kobune, K. (1988). Directional spectrum estimation from a bayesian approach. *Coastal Engineering Proceedings*, **1(21),4**, 62–76.

Hashimoto, N., Nagai, T. and Asai, T. (1994). Extension of the maximum entropy principle method for directional wave spectrum estimation. *Proceedings of 24th International Conference on Coastal Engineering, Kobe, Japan*, 232–246.

Haubrich, R.A. (1968). Array design. *Bulletin of the Seismological Society of America*, **58 (3)**, 977–991.

Hawkes, P.J., Ewing, J.A., Harford, C.M., Klopman, G., Stansberg, C.T., Benoit, M., Briggs, M.J., Frigaard, P., Hiraishi, T., Miles, M., Santas, J. and Schäffer, H.A. (1997). Comparative analysis of multidirectional wave basin data. *IAHR Seminar on Multidirectional Waves and their Interaction with Structures.*

Isobe, M., Kondo, K. and Horikawa, K. (1984). Extension of mlm for estimating directional wave spectrum. *Proc. Sympo. On Description and Modelling of Directional Seas*, **A-6**.

Iversen, S.K., Andersen, T.L. and Frigaard, P. (2023). Accuracy of directional spectrum estimation in 2nd order multidirectional waves. *Proceedings of the Thirty-third International Ocean and Polar Engineering Conference*, 2395–2402. DOI: onepetro.org/ISOPEIOPEC/proceedings-abstract/ISOPE23/All-ISOPE23/ISOPE-I-23-346/524699?redirectedFrom=PDF.

Krogstad, H.E. (1988). Maximum likelihood estimation of ocean wave spectra from general arrays of wave gauges. *Modelling, Identification and Control*, **9**, 373–381.

Lin, C.Y. and Huang, C.J. (2004). Decomposition of incident and reflected higher harmonic waves using four wave gauges. *Coastal Engineering*, **51**, 395–406. DOI: 10.1016/j.coastaleng.2004.04.004.

Mansard and Funke (1980). The measurement of incident and reflected spectra using a least squares method. *Proceedings of the 17th Coastal Engineering Conference, New York, USA*, 154–172.

Mitsuyasu, H., Tasai, F., Suhara, T., Mizuno, S., Onkusu, M., Honda, T. and Rukiiski, K. (1975). Observations of the directional spectrum of ocean waves using a cloverleaf buoy. *J. Phys. Oceanogr.*, **5**, 751–761.

Nelder, J.A. and Mead, R. (1965). A simplex method for function minimization. *The Computer Journal*, **7,4**, 308–313.

Padilla, E.M. and Alsina, J.M. (2020). A general framework for wave separation in the frequency domain. *Coastal Engineering*, **158**.

Wenneker, I. and Hofland, B. (2014). Optimal wave gauge spacings for separation of incoming and reflected waves. *Proceedings on the Fifth International Conference on the Application of Physical Modelling to Port and Coastal Protection (Coastlab), Varna, Bulgaria.*

Zelt, J.A. and Skjelbreia, J.E. (1992). Estimating incident and reflected wave fields using an arbitrary number of wave gauges. *Proceedings of 23rd Conference on Coastal Engineering, Venice, Italy*, 777–789.